energies

MDPI

*Article*

# Experimental Analysis of the Long-Term Stability of Thermoelectric Generators under Thermal Cycling in Air and Argon Atmosphere

**Julian Schwab *, Christopher Fritscher, Michael Filatov, Martin Kober, Frank Rinderknecht and Tjark Siefkes**

German Aerospace Center (DLR), Institute of Vehicle Concepts, 70569 Stuttgart, Germany
* Correspondence: julian.schwab@dlr.de

**Abstract:** It is estimated that 72% of the worldwide primary energy consumption is lost as waste heat. Thermoelectric Generators (TEGs) are a possible solution to convert a part of this energy into electricity and heat for space heating. However, for their deployment a proven long-term operation is required. Therefore, this research investigates the long-term stability of TEGs on system level in air and argon atmosphere under thermal cycling up to 543 K. The layout of the examined test objects resembles a TEG in stack design. The results show that the maximal output power of the test object in air reaches a plateau at 57% of the initial power after 50 cycles caused by an increased electrical resistance of the system. Whereas the test object in argon atmosphere shows no significant degradation of electrical power or resistance. The findings represent a step towards the understanding of the long-term stability of TEGs and can be used as a guideline for design decisions.

**Keywords:** thermoelectric; generator; module; half-Heusler; long-term stability



**Citation:** Schwab, J.; Fritscher, C.; Filatov, M.; Kober, M.; Rinderknecht, F.; Siefkes, T. Experimental Analysis of the Long-Term Stability of Thermoelectric Generators under Thermal Cycling in Air and Argon Atmosphere. *Energies* **2023**, *16*, 4145. https://doi.org/10.3390/en16104145

Academic Editor: Diana Enescu

Received: 23 March 2023
Revised: 28 April 2023
Accepted: 29 April 2023
Published: 17 May 2023



## 1. Introduction

The improvement of the energy efficiency of various technical processes is an essential objective in the commercial and private sector. It reduces emissions of greenhouse gases, counteracts rising energy costs and enables the adherence to legal requirements. Thermal processes have a high potential for efficiency improvements. They are used for processing heat, home heating systems, stationary and mobile internal combustion engines and other uses. It is estimated that currently 72% of the worldwide primary energy consumption is lost as waste heat [1]. Efforts for waste heat recovery are often abandoned due to the complexity or the investment costs of the available systems.

Thermoelectric Generators (TEGs) are a possible solution to recover a higher share of the waste heat. They work according to the Seebeck effect. It describes two dissimilar conductors which are connected electrically in series and thermally in parallel. When the junctions are maintained at a temperature difference an electrical potential across the conductors develops [2]. To utilize this effect, legs of p- and n-type semiconductors are electrically connected and assembled on electric isolators. The assembled devices are Thermoelectric Modules (TEMs). The thermoelectric efficiency of these semiconducting materials is classified by the figure of merit

$$ZT = \frac{\alpha^2 \sigma}{\lambda} T \tag{1}$$

with the differential Seebeck-coefficient $\alpha$ in $VK^{-1}$, the electrical conductivity $\sigma$ in $Sm^{-1}$, the thermal conductivity $\lambda$ in $Wm^{-1}K^{-1}$ and the temperature in K [2]. For low temperature applications below 600 K commonly used materials are based on bismuth telluride (BiTe). For applications with higher temperatures, the materials used include lead telluride (PbTe), Skutterudites or half-Heusler compounds. Other materials in the medium temperature region, such as copper sulfide compounds, are currently under development [3].

TEGs are systems consisting of TEMs between the hot side and cold side heat exchangers as shown in Figure 1. They can be integrated in waste heat flows, where the waste heat is absorbed by the hot side heat exchanger and transferred through the TEMs to a fluid in the cold side heat exchangers. In this way electrical energy is produced and additionally in stationary applications the heat in the fluid can be used for space heating. TEGs do not need any moving parts and are therefore low-maintenance and low-noise, compact, and have potentially low investment costs. They are suitable for a variety of applications, with economic benefits even with low to medium amounts of waste heat. Their potential is shown by Kober et al. [4,5] for passenger vehicles, by Heber et al. [6,7] for commercial vehicles and by Schwab et al. [8] for cogeneration in residential heating systems.

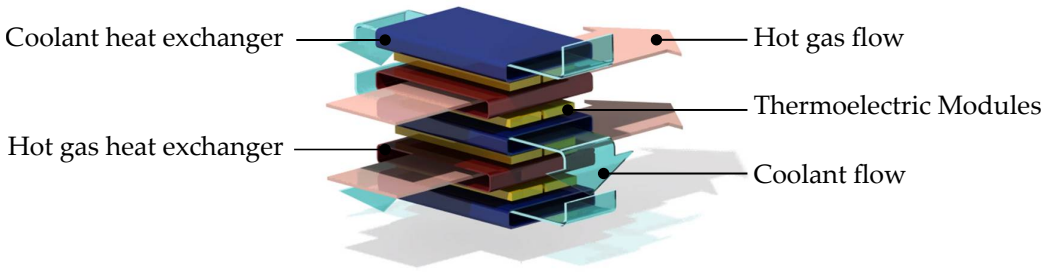


**Figure 1.** Concept of a stackable TEG design in crossflow arrangement [4]. The heat is transferred from the hot gas flow through the Thermoelectric Modules to the coolant flow with the heat exchangers.

An important criterion for the application of TEGs is their long-term stability. It influences their economic benefits and emission reduction potential. Ageing mechanisms of thermoelectric materials are sublimation, oxidation, diffusion processes, mechanical damaging and others. The processes depend on various characteristics, such as the material class and composition, geometry and external conditions. Parameters that influence the long-term stability are their maximal operational temperature, cycling of the temperature, including amplitude and heating rate of the cycles, mechanical parameters, such as compression pressure, or the atmosphere around the TEMs. They impact the thermoelectric properties and therefore the efficiency. Possible prevention strategies include coating of the materials and electrodes, sealing of the TEMs or the operation in a non-reactive atmosphere like vacuum or argon.

Sublimation is the phase change from solid to gaseous state and often degrades thermoelectric material at high temperatures. Sublimation rates of PbTe and PbSnTe increase with the temperature as measured by Bates and Weinstein in vacuum at temperatures of 673 K and 873 K [9]. Similar behavior is reported by Ohsugi et al. for other telluride-based materials. Telluride is dissociated and agglomerates at the surface of the material where it sublimates at temperatures above 673 K [10]. Skutterudites based on $CoSb_3$ also show thermal degradation. The material in varying atmospheres including vacuum, helium and air at temperatures of 293 K to 1123 K is investigated by Leszczynski et al. [11] and Broz et al. [12]. The $CoSb_3$ is stable at temperatures to around 873 K, above this temperature CoSb2 dissociates to the surface and eventually CoSb dissipates. Half-Heusler compounds are reported to be more stable. Experiments by Zelenka et al. with TiFe1.33Sb and $Ti_xNb_{1-x}FeSb$ show very low sublimation of Sb at temperatures to 873 K in an Argon atmosphere [13].

Oxidation of thermoelectric materials is their reaction with oxygen from surrounding air. For PbTe-based materials, models by Berchenko et al. show that $PbTeO_3$ already starts to form at temperatures of 673 K [14]. The influence of the partial pressure of oxygen on the oxidation of PbTe is analyzed by Chen et al. With a rising partial pressure, the oxidation rate rises as well [15]. Skutterudites are also affected by oxidation. This is reported for $CeFe_4Sb_{12}$ and $YbyCo_4Sb_{12}$ at temperatures over 573 K and 650 K, respectively, by Sklad et al. [16] and Xia et al. [17,18]. To reduce the oxidation of $CoSb_3$, different

coatings are investigated by Skomedal et al. and $Al_2O_3$ is found to be effective with reduced oxidation at 180 thermal cycles to 873 K [19]. Another possibility to reduce the oxidation is by altering the surrounding atmosphere. $La_{0.9}Fe_3CoSb_{12}$ oxidizes on air at temperatures above 673 K, this is prevented by Shin et al. with a vacuum atmosphere and no oxidation is found while tempering the material at 823 K for 100 h [20]. Half-Heusler alloys oxidize at higher temperatures. Different material compositions, such as MNiSn, MCoSb with M = Hf, Zr or Ti and NbSeSb at 873 K for 168 h are investigated by Kang et al. MNiSn and NbSeSb show a higher stability of less than 7% then MCoSb [21]. At even higher temperatures of 1000 K, oxidation of TiNiSn to $TiO_2$ and $Ti_2O_3$ [22] and of ZrNiSn to $ZrO_2$ is found by Appel et al. [23]. Similar behavior is also reported by Zillmann et al. for the commercial materials $Zr_{0.5}Hf_{0.5}CoSb_{0.8}Sn_{0.2}$, $Zr_{0.25}Hf_{0.25}Ti_{0.5}NiSn$ and $Zr_{0.4}Hf_{0.6}NiSn_{0.98}Sb_{0.02}$. It oxidizes in an air atmosphere at 1073 K and is stable in an Argon atmosphere [24].

Diffusion processes occur inside of the materials and especially at the contact interfaces to the electrodes. These processes for PbTe and $Pb_{0.6}Sn_{0.4}Te$ in combination with copper and silver electrodes at temperatures of 673 K for 1000 h and 773 K for 50 h are analyzed by Li et al. It shows that $Pb_{0.6}Sn_{0.4}Te$ reacts with both electrode materials even at low temperatures, but the contact of the PbTe is uniform and with no crack formation. However, copper diffuses in the leg and affects the thermoelectric properties [25]. To reduce this, it is possible to apply a diffusion barrier at the contact interface. A NiTe-layer is used and no diffusion while tempering the material at 823 K for 360 h in vacuum is observed by Ferres et al. [26]. Diffusion barriers are also used for skutterudite materials. CoMo is used by Feng et al. [27] and Nb is used by Chu et al. [28] as a metallization layer on $CoSb_3$ and no significant diffusion during testing is found. A direct bonding method for ZrCoSb- and ZrNiSn-based half-Heusler materials is used by Nozariasbmarz et al. High efficiencies of over 9.5% and a performance reduction of 2.7% after tempering the material at 823 K for 20 h is achieved [29].

The combination of mechanical loads and high temperatures, both often in a cyclic manner, results in mechanical damages such as crack formation, creep or direct mechanical failure. The resulting effects are studied by Al Malki et al. for a ZrNiSn-based half-Heusler alloy. When compressed at a temperature of 873 K, it shows no macroscopic failure or creep, but the beginning of crack formation [30].

In addition to the research on material level, the analysis of the long-term stability on TEM level is also relevant. It expands the scope, including the geometry of the module, implications of the production processes and the interactions of the electric isolators, electrodes and thermoelectric legs. Most studies are conducted regarding BiTe-TEM of different manufacturers, as these are the most commonly available type. Ding et al. [31] find that the power reduces by 37% after 7 h at 483 K, Harish et al. [32] obtain similar results after 300 thermal cycles. Riyadi et al. investigate different thermal cycling heating rates and find that the electrical resistance of the TEM rises with higher heating rates [33]. Merienne et al. also investigate different heating rates but with sealed TEMs. They still find a significant power loss and a correlation to the heating rates [34]. Barako et al. cycle from 253 K to 419 K for 45,000 cycles. The effective figure of merit reduces after 40,000 cycles by 20% and after 45,000 cycles by 97%. The reason is a higher electrical resistance due to crack formation [35]). Salvador et al. investigate PbTe- and $CoSb_3$-based high temperature TEMs sealed with aerogel. The TEMs are exposed to cyclic temperatures from 300 K to 673 K and 723 K and tempered for 200 h at 698 K and 750 K, respectively. The PbTe-based TEMs display a lower long-term stability compared to the $CoSb_3$-based TEMs. They show signs of interlayer diffusion, sublimation and oxidation of the material and the electrical connections [36].

The mentioned research focuses on the long-term stability of thermoelectric materials and modules. However, there is no research on the long-term stability on the system level of TEGs, including TEMs, heat exchangers and structural components, such as compression bolts and plates. This is important for applications because it takes additional effects into

account. On the system-level, the mechanical degradation resistance of all components affects the overall performance. Creep or crack formation may result in a lower contact pressure or leaks in the inert gas housing. Furthermore, the loads on the TEMs have not been studied in an application-orientated environment with inhomogeneous temperature gradients or pressure distribution.

Therefore, this research focuses on the long-term stability of TEGs on system-level. The aim is to investigate how the atmosphere influences the long-term stability of such systems in an application-orientated test. This is particularly interesting, as systems with air atmosphere are less complex. Additional factors which are relevant for an application of the systems are represented. The test objects are based on the geometry of TEGs and are able to replicate realistic loads. In line with this, the temperature load is applied cyclically as in most waste heat recovery applications. The evaluation is also system-orientated as the primarily considered parameter is the power output of the system and its long-term progress. The first tests are designed to determine the possibility to systematically improve the power output stability with an argon inert gas atmosphere. The findings can be used for the design process of future TEGs and develop them further towards deployment.

## 2. Methodology

The layout of the test objects is shown in Figure 2, it is based on a stackable TEG design. The heat is generated by electrical heating cartridges which are embedded in a plate. The cartridges have a maximum operation temperature of 1023 K and a total heat power of 10 kW. On one side of the heating plate is an isolating layer and on the other side a steel sheet with grooves on the surface. For the experiment type K thermocouples are placed in the grooves to measure the surface temperature of the TEMs. Six TEMs are electrically connected in series and placed on the steel sheet. The TEMs are based on (Ti,Zr)NiSn for the n-type and FeNbSb for the p-type and produced by the professional manufacturer Yamaha Corporation. The material is chosen as it has a high maximal temperature, a ZT value of around unity and a high mechanical stability. Each TEM has a nominal power output of 46.1 $W^{el}$ at 450 K temperature difference and an active area of around 1453 $mm^2$. The TEMs are connected with soldered copper cables. Above the TEMs is a coolant heat exchanger as heat sink. It also has grooves on the surface for thermocouples to measure the cold side temperature of the TEMs. The whole stack is compressed to around two MPa pressure on the TEMs with a structure consisting of two stiff compression plates and four compression bolts. The applied pressure and graphite sheets between each layer are needed to minimize the thermal contact resistance between the components.

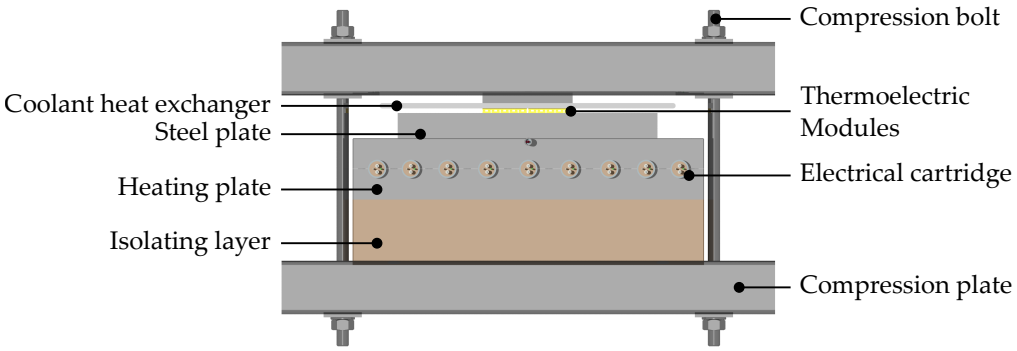


**Figure 2.** Schematic view of the layout of the test objects. The Thermoelectric Modules are compressed with a compression structure to a heating plate and a coolant heat exchanger.

The experimental setting consists of two identical test objects, which are only distinguishable by their production tolerance. One heating plate is produced with a more accurate tolerance and is thus able to absorb the heat of the cartridges slightly more efficiently. The test objects are placed in gas tight chambers, as shown in Figure 3. One chamber is filled with argon at around 1.5 bar absolute pressure, the other one is open and the test

object is exposed to ambient air. The argon concentration of the argon filled chamber is monitored with a lambda probe and its pressure is monitored with an absolute pressure sensor. On the coolant side, the test objects are connected to a temperature control unit with a heat sink. The control unit is able to set the required mass flow and inlet temperature of the water that is used as coolant. The temperature is measured with Pt100 senors in a four wire arrangement in the cooling unit and additionally type K thermocouples directly at the inlet and outlet of the test chambers. Moreover, thermocouples are placed in various places throughout the experimental setup to measure if the system is overheating and to switch off the process. This is particularly important for an automatic procedure.

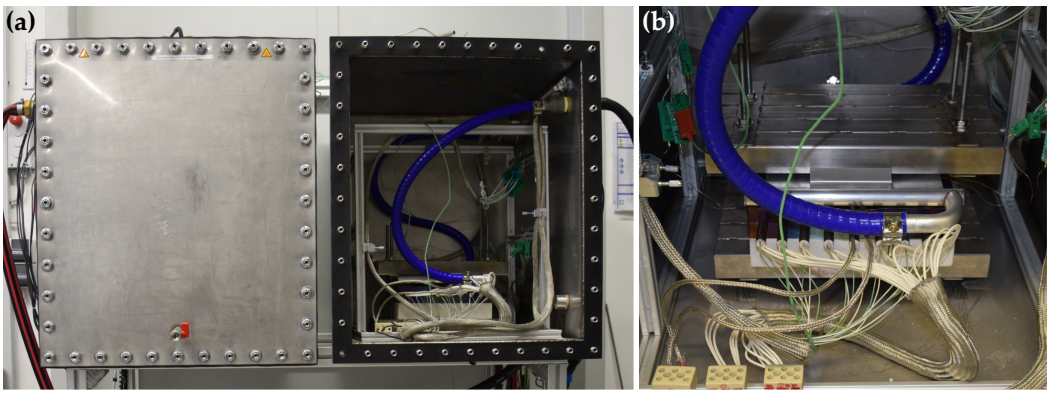


**Figure 3.** View of the experimental setup: (**a**) Test bench with the closed test chamber filled with argon and the open test chamber. (**b**) Test object in the test chamber.

The TEMs of each test object are connected to a self-developed maximum power point tracker (MPPT). It adjusts the outer electrical resistance of the electrical load to the inner electrical resistance of the TEMs in order to maximize their power output. The tracking algorithm increases and decreases the electrical current on a fixed frequency and adjusts the current accordingly. Other algorithms, such as shuffled frog leaping algorithm [37] or selective harmonic elimination [38], are currently not used. The MPPT has integrated precision resistances for the measurement of voltage and current. The measured values are transferred to the measurement system and are recorded there. The measurement system consists of ProfiMessage data acquisition modules from Delphin Technology. All measured values are supplied by the sensors as an electrical signal. The signal is transferred from the sensor to the measuring device, where it is converted to a digital signal and recorded. This measurement chain is calibrated with a Beamex MC2 device. The output power of the test objects is calculated by multiplying the output voltage and current at the maximum power point. The electrical resistance is calculated by Ohm's law.

For thermal cycling, the cartridges of the first test object start to heat with maximum power until their temperature limit is reached. When their maximum temperature is reached, they are controlled with a pulse-width modulation to keep the temperature constant and to allow a stationary thermal state. During heating, the coolant flow is set to 25 L/min at a temperature of 333 K. When the stationary state is reached, the cartridges stop to heat and the coolant flow is set to 40 L/min at 293 K until the mean cold side temperature is 323 K. Afterwards the heating of the second test object starts in the same pattern. The resulting temperatures are shown in Figure 4. Because of the different production tolerances of the heating plates, the temperature curve and maximum temperature of the test object in air is slightly higher compared to the test object in argon. For the same reason, the heating duration of the test object in air is 34 min and for the one in argon is 43 min. The duration of one complete cycle is around 95 min.

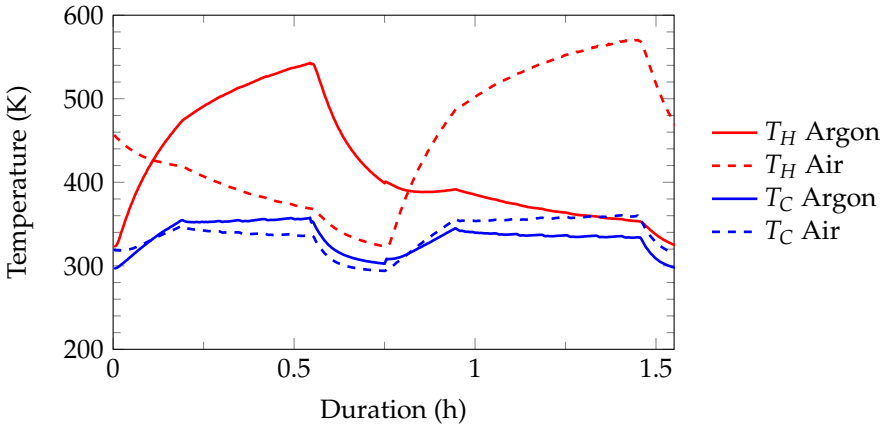


**Figure 4.** Temperature profiles of the hot and cold side of the test objects in air and argon. One test object is heated while the other test object is cooled and vice versa.

## 3. Results and Discussion

The thermal cycles are performed until a plateau of the maximum output power is reached. For each cycle, the electric parameters at the maximum power point is measured at a hot side temperature of 543 K. This is the highest hot side temperature both test objects reach during the tests. The results of these measurements are shown in Figure 5. They normalized on the initial values to make them comparable. The initial maximum power of the test object in air is 57.2 W and of the test object in argon is 68.5 W. The initial offset is caused by the differences in production and assembly of the test objects and its components. The pressure and oxygen level of the argon atmosphere is monitored during the experiment and argon is refilled to the initial values when the oxygen level exceeds 5%. The initial values are 1.25 bar and 0.8%, respectively.

The maximum power of the test object in air atmosphere steadily decreases until it reaches a plateau at around 57% of its initial maximum power after around 50 cycles. The course of the measured values of the test object in argon atmosphere shows no steady degradation. After the cycles two and nine, there are abrupt drops in performance, and after cycle 16, there is a shortcut in the system and the power drops significantly. This is caused by a contact of the thermal interface material with the electrodes. At cycle 22, the shortcut is manually removed and the test object returns to operation at around 95% of its initial maximum power with no additional degradation during the subsequent cycles.

Figure 5 shows that the power performance output reduction of the test object in air is caused by an increasing inner resistance from 5.13 Ω to 9.24 Ω and a corresponding decrease in electrical current from 3.38 A to 1.95 A while the voltage is roughly constant at about 16.9 V. Similar to the progression of the power, the electrical values of the test object in argon show no degradation and only the changes due to the shortcut in the system are observable. The inner resistance rises by 4.38% from 4.34 Ω to 4.53 Ω, the voltage rises by 0.12% from 16.95 V to 16.97 V and the current declines by 4.95% from 4.04 A to 3.84 A.

The results show that an air atmosphere causes significantly reduced long-term stability of TEGs compared to the use of an argon atmosphere as inert gas. Although the Seebeck coefficient is not influenced by the air atmosphere for over 50 cycles, the increase of inner resistance leads to a power decrease. Based on the literature on long-term stability of Thermoelectric Modules, important degradation mechanisms are oxidation and crack formation, or a combination of both, on the material and especially at the interfaces to the electrodes; these effects are also found in literature [24]. In Argon gas, there is no oxygen that reacts with the material and causes oxidation; therefore, this effect is limited. Furthermore, the combination of cracking and oxidation in the cracks is limited as well. The mechanical components of the system consisting of the compression bolts, compression plate, and hot and cold side heat exchangers show no degradation during the experiment

and there is no positive or negative influence of the overall mechanical system on the long-term stability detected during the measurements.

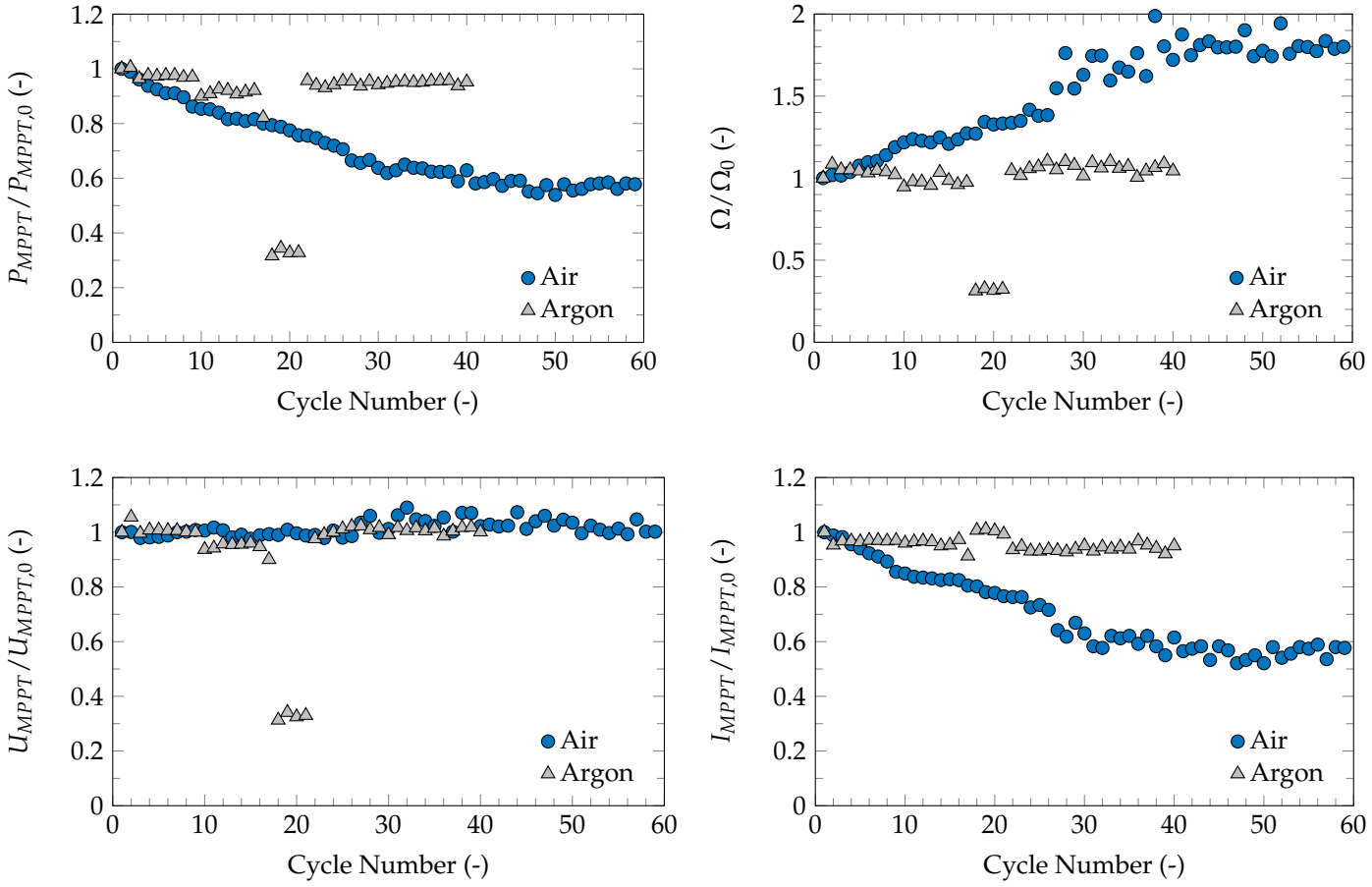


**Figure 5.** Progression of the electrical parameters power, inner resistance, voltage and current of the test obejts in air and argon. All values are at the maximum power point and normalized to the inital value.

The experiment is designed to represent a real application of TEGs. However, some simplifications are needed for an efficient experimental procedure, that differ to the final applications. These simplifications include a non-symmetry of the stack, as the TEMs are only on one side of the heating plate, the absence of exhaust gas in the hot gas heat exchanger, which may affect its long-term behavior or the absence of the housing, which may also be subject to degradation. Moreover, although the results are already significant, the test procedure should be repeated with the same parameters in order to specify statistic influences, which are based on production tolerances, for example.

The experiment shows the need of an inert gas atmosphere for the successful operation of TEGs with commercially produced high-temperature Thermoelectric Modules. To further understand the systems, experiments with a broader variety of Thermoelectric Modules from different manufacturers or research institutions are needed. Furthermore, future experiments are planned to perform more cycles and to study the influence of parameters such as maximal temperature, cycle duration and oxygen concentration. After future experiments with a higher number of cycles, the Thermoelectric Modules and the overall system should be examined, especially regarding microcrack formation. This research represents a step towards the understanding of the long-term stability of TEGs and can be used as a guideline for design decisions.

## 4. Conclusions

TEGs are a possible solution to recover waste heat from various processes and to reduce the process costs and emissions. This research aims to investigate their degradation on system level and a possible approach to minimize the degradation. An experiment on two test objects with high-temperature, professionally produced Thermoelectric Modules in air and in argon atmosphere is performed. Their layout is based on a stackable TEG design and resembles its technological features. The hot-side temperature of the test objects is increased to around 543 K and then decreased to 332 K in a cyclic manner. The output power at the maximum power point and the electrical parameters of the test objects are measured.

The results show a significant reduction of the maximal output power of the test object in air reaching a plateau at around 57% of its initial maximum power after 50 cycles. The argon atmosphere shows a positive influence on the degradation behavior, as the output power remains constant during the cyclic tests. In both test objects the voltage is at a constant level, but in air, the inner resistance increases and the current decreases accordingly. Therefore, the increase of the inner resistance leads to the decrease of the output performance. A comparison with the literature shows that oxidation and crack formation on the material and especially at the interfaces to the electrodes are the main reasons for the degradation.

In future experiments, different Thermoelectric Modules from various producers and the influence of test parameters such as cycle duration, maximal temperature and oxygen concentration should be considered. The selection of the different Modules should be based on their maximal temperature, as the long-term stability in the high temperature regime is especially critical. Promising material classes for this investigation are Half-Heusler alloys and Skutterudites. After the experiments, all components should be examined regarding microcrack formation. To consolidate research about this topic, standard testing procedures may be introduced that are based on application-orientated thermal cycles. This research represents a step towards the understanding of the long-term stability of TEGs on system level and can be used as a guideline for design decisions.

**Author Contributions:** Conceptualization, J.S., C.F. and M.F.; methodology, J.S., C.F. and M.F.; software, J.S., C.F. and M.F.; validation, J.S., C.F. and M.F.; formal analysis, C.F. and M.F.; investigation, J.S., C.F. and M.F.; resources, J.S., C.F., M.F.; data curation, J.S., C.F. and M.F.; writing—original draft preparation, J.S.; writing—review and editing, J.S., C.F., M.F., M.K., F.R. and T.S.; visualization, J.S.; supervision, M.K., F.R. and T.S.; project administration, J.S.; funding acquisition, J.S., M.K., F.R. and T.S. All authors have read and agreed to the published version of the manuscript.

**Funding:** This research was externally funded by the Federal Ministry for Economic Affairs and Climate Action in the project RecoveryPlus, grant number 03EN2024A.

**Data Availability Statement:** The data presented in this study are available on request from the corresponding author. The data are not publicly available due to privacy reasons.

**Acknowledgments:** The authors acknowledge the support and cooperation with all external and internal partners and appreciate their contributions to this work. Especially Takahiro Hayashi from Yamaha Corporation for the helpful discussions and support regarding the thermoelectric modules.

**Conflicts of Interest:** The authors declare no conflict of interest.

## Abbreviations

The following abbreviations are used in this manuscript:

| | |
|---|---|
| BiTe | Bismuth telluride |
| C | Cold side |
| H | Hot side |
| MPPT | Maximum power point tracker |
| PbTe | Lead telluride |
| TEG | Thermoelectric Generator |
| TEM | Thermoelectric Module |

## References


1. Forman, C.; Muritala, I.K.; Pardemann, R.; Meyer, B. Estimating the global waste heat potential. *Renew. Sustain. Energy Rev.* **2016**, *57*, 1568–1579. [CrossRef]
2. Rowe, D.M. (Ed.) *Thermoelectrics Handbook: Macro to Nano*; CRC/Taylor & Francis: Boca Raton, FL, USA, 2006.
3. Chen, X.Q.; Fan, S.J.; Han, C.; Wu, T.; Wang, L.J.; Jiang, W.; Dai, W.; Yang, J.P. Multiscale architectures boosting thermoelectric performance of copper sulfide compound. *Rare Met.* **2021**, *40*, 2017–2025. [CrossRef] [PubMed]
4. Kober, M. Holistic Development of Thermoelectric Generators for Automotive Applications. *J. Electron. Mater.* **2020**, *49*, 2910–2919. [CrossRef]
5. Kober, M.; Knobelspies, T.; Rossello, A.; Heber, L. Thermoelectric Generators for Automotive Applications: Holistic Optimization and Validation by a Functional Prototype. *J. Electron. Mater.* **2020**, *49*, 2902–2909. [CrossRef]
6. Heber, L.; Schwab, J. Modelling of a thermoelectric generator for heavy-duty natural gas vehicles: Techno-economic approach and experimental investigation. *Appl. Therm. Eng.* **2020**, *174*, 115156. [CrossRef]
7. Heber, L.; Schwab, J.; Knobelspies, T. 3 kW Thermoelectric Generator for Natural Gas-Powered Heavy-Duty Vehicles—Holistic Development, Optimization and Validation. *Energies* **2022**, *15*, 15. [CrossRef]
8. Schwab, J.; Bernecker, M.; Fischer, S.; Seyed Sadjjadi, B.; Kober, M.; Rinderknecht, F.; Siefkes, T. Exergy Analysis of the Prevailing Residential Heating System and Derivation of Future $CO_2$-Reduction Potential. *Energies* **2022**, *15*, 3502. [CrossRef]
9. Bates, H.E.; Weinstein, M. Sublimation rates In vacuo of PbTe and $Pb_{0.5}Sn_{0.5}Te$ thermoelements. *Adv. Energy Convers.* **1966**, *6*, 177–180. [CrossRef]
10. Ohsugi, I.J.; Tokunaga, D.; Kato, M.; Yoneda, S.; Isoda, Y. Dissociation and sublimation of tellurium from the thermoelectric tellurides. *Mater. Res. Innov.* **2015**, *19*, S5-301–S5-303. [CrossRef]
11. Leszczynski, J.; Wojciechowski, K.T.; Malecki, A.L. Studies on thermal decomposition and oxidation of CoSb3. *J. Therm. Anal. Calorim.* **2011**, *105*, 211–222. [CrossRef]
12. Brož, P.; Zelenka, F.; Kohoutek, Z.; Vřešťál, J.; Vykoukal, V.; Buršík, J.; Zemanová, A.; Rogl, G.; Rogl, P. Study of thermal stability of CoSb3 skutterudite by Knudsen effusion mass spectrometry. *Calphad* **2019**, *65*, 1–7. [CrossRef]
13. Zelenka, F.; Brož, P.; Vřešťál, J.; Buršík, J.; Zemanová, A.; Rogl, G.; Rogl, P. Study of thermal stability of half-Heusler alloys TiFe1.33Sb and TixNb1-xFeSb (x = 0, 0.15) by differential thermal analysis and Knudsen effusion method. *Calphad* **2021**, *74*, 102292. [CrossRef]
14. Berchenko, N.; Fadeev, S.; Savchyn, V.; Kurbanov, K.; Trzyna, M.; Cebulski, J. Pb–Te–O phase equilibrium diagram and the lead telluride thermal oxidation. *Thermochim. Acta* **2014**, *579*, 64–69. [CrossRef]
15. Chen, L.; Goto, T.; Tu, R.; Hirai, T. High-temperature Oxidation Behavior Of PbTe And Oxidation-resistive Glass Coating. In Proceedings of the 16th International Conference on Thermoelectrics (1997), Dresden, Germany, 26–29 August 1997.
16. Sklad, A.C.; Gaultois, M.W.; Grosvenor, A.P. Examination of CeFe4Sb12 upon exposure to air: Is this material appropriate for use in terrestrial, high-temperature thermoelectric devices? *J. Alloys Compd.* **2010**, *505*, L6–L9. [CrossRef]
17. Xia, X.; Qiu, P.; Shi, X.; Li, X.; Huang, X.; Chen, L. High-Temperature Oxidation Behavior of Filled Skutterudites Yb y Co4Sb12. *J. Electron. Mater.* **2012**, *41*, 2225–2231. [CrossRef]
18. Xia, X.; Qiu, P.; Huang, X.; Wan, S.; Qiu, Y.; Li, X.; Chen, L. Oxidation Behavior of Filled Skutterudite CeFe4Sb12 in Air. *J. Electron. Mater.* **2014**, *43*, 1639–1644. [CrossRef]
19. Skomedal, G.; Kristiansen, N.R.; Engvoll, M.; Middleton, H. Methods for Enhancing the Thermal Durability of High-Temperature Thermoelectric Materials. *J. Electron. Mater.* **2014**, *43*, 1946–1951. [CrossRef]
20. Shin, D.K.; Kim, I.H.; Park, K.H.; Lee, S.; Seo, W.S. Thermal Stability of La0.9Fe3CoSb12 Skutterudite. *J. Electron. Mater.* **2015**, *44*, 1858–1863. [CrossRef]
21. Kang, H.B.; Saparamadu, U.; Nozariasbmarz, A.; Li, W.; Zhu, H.; Poudel, B.; Priya, S. Understanding Oxidation Resistance of Half-Heusler Alloys for in-Air High Temperature Sustainable Thermoelectric Generators. *ACS Appl. Mater. Interfaces* **2020**, *12*, 36706–36714. [CrossRef]
22. Appel, O.; Cohen, S.; Beeri, O.; Shamir, N.; Gelbstein, Y.; Zalkind, S. Surface Oxidation of TiNiSn (Half-Heusler) Alloy by Oxygen and Water Vapor. *Materials* **2018**, *11*, 2296. [CrossRef]
23. Appel, O.; Breuer, G.; Cohen, S.; Beeri, O.; Kyratsi, T.; Gelbstein, Y.; Zalkind, S. The Initial Stage in Oxidation of ZrNiSn (Half Heusler) Alloy by Oxygen. *Materials* **2019**, *12*, 1509. [CrossRef]
24. Zillmann, D.; Waag, A.; Peiner, E.; Feyand, M.H.; Wolyniec, A. Thermoelectric and Structural Properties of Zr-/Hf-Based Half-Heusler Compounds Produced at a Large Scale. *J. Electron. Mater.* **2018**, *47*, 1546–1554. [CrossRef]
25. Li, C.C.; Drymiotis, F.; Liao, L.L.; Hung, H.T.; Ke, J.H.; Liu, C.K.; Kao, C.R.; Snyder, G.J. Interfacial reactions between PbTe-based thermoelectric materials and Cu and Ag bonding materials. *J. Mater. Chem. C* **2015**, *3*, 10590–10596. [CrossRef]
26. Ferreres, X.R.; Aminorroaya Yamini, S.; Nancarrow, M.; Zhang, C. One-step bonding of Ni electrode to n-type PbTe—A step towards fabrication of thermoelectric generators. *Mater. Des.* **2016**, *107*, 90–97. [CrossRef]
27. Feng, H.; Zhang, L.; Zhang, J.; Gou, W.; Zhong, S.; Zhang, G.; Geng, H.; Feng, J. Metallization and Diffusion Bonding of CoSb3-Based Thermoelectric Materials. *Materials* **2020**, *13*, 1130. [CrossRef]
28. Chu, J.; Huang, J.; Liu, R.; Liao, J.; Xia, X.; Zhang, Q.; Wang, C.; Gu, M.; Bai, S.; Shi, X.; et al. Electrode interface optimization advances conversion efficiency and stability of thermoelectric devices. *Nat. Commun.* **2020**, *11*, 2723. [CrossRef]

29. Nozariasbmarz, A.; Saparamadu, U.; Li, W.; Kang, H.B.; Dettor, C.; Zhu, H.; Poudel, B.; Priya, S. High-performance half-Heusler thermoelectric devices through direct bonding technique. *J. Power Sources* **2021**, *493*, 229695. [CrossRef]
30. Al Malki, M.M.; Qiu, Q.; Zhu, T.; Snyder, G.J.; Dunand, D.C. Creep behavior and postcreep thermoelectric performance of the n-type half-Heusler alloy Hf0.3Zr0.7NiSn0.98Sb0.02. *Mater. Today Phys.* **2019**, *9*, 100134. [CrossRef]
31. Ding, L.C.; Akbarzadeh, A.; Date, A. Performance and reliability of commercially available thermoelectric cells for power generation. *Appl. Therm. Eng.* **2016**, *102*, 548–556. [CrossRef]
32. Harish, S.; Sivaprahasam, D.; Jayachandran, B.; Gopalan, R.; Sundararajan, G. Performance of bismuth telluride modules under thermal cycling in an automotive exhaust thermoelectric generator. *Energy Convers. Manag.* **2021**, *232*, 113900. [CrossRef]
33. Riyadi, T.W.B.; Utomo, B.R.; Effendy, M.; Wijayanta, A.T.; Al-Kayiem, H.H. Effect of thermal cycling with various heating rates on the performance of thermoelectric modules. *Int. J. Therm. Sci.* **2022**, *178*, 107601. [CrossRef]
34. Merienne, R.; Lynn, J.; McSweeney, E.; O'Shaughnessy, S.M. Thermal cycling of thermoelectric generators: The effect of heating rate. *Appl. Energy* **2019**, *237*, 671–681. [CrossRef]
35. Barako, M.T.; Park, W.; Marconnet, A.M.; Asheghi, M.; Goodson, K.E. Thermal Cycling, Mechanical Degradation, and the Effective Figure of Merit of a Thermoelectric Module. *J. Electron. Mater.* **2013**, *42*, 372–381. [CrossRef]
36. Salvador, J.R.; Cho, J.Y.; Ye, Z.; Moczygemba, J.E.; Thompson, A.J.; Sharp, J.W.; König, J.D.; Maloney, R.; Thompson, T.; Sakamoto, J.; et al. Thermal to Electrical Energy Conversion of Skutterudite-Based Thermoelectric Modules. *J. Electron. Mater.* **2013**, *42*, 1389–1399. [CrossRef]
37. Siadatan, A.; fakhari, M.; Taheri, B.; Sedaghat, M. New fundamental modulation technique with SHE using shuffled frog leaping algorithm for multilevel inverters. *Evol. Syst.* **2020**, *11*, 541–557. [CrossRef]
38. Torkaman, H.; Fakhari, M.; Karimi, H.; Taheri, B. New Frequency Modulation Strategy with SHE for H-bridge Multilevel Inverters. In Proceedings of the 2018 4th International Conference on Electrical Energy Systems (ICEES), Chennai, India, 7–9 February 2018; pp. 157–161. [CrossRef]